Acoustic Cavitation at the Water−Glass Interface

ARTICLE *in* THE JOURNAL OF PHYSICAL CHEMISTRY C · AUGUST 2010

Impact Factor: 4.77 · DOI: 10.1021/jp1046276 · Source: OAI

Acoustic Cavitation at the Water−Glass Interface

Matthieu Virot,[†] Tony Chave,[†] Sergey I. Nikitenko,*[,†] Dmitry G. Shchukin,[‡] Thomas Zemb,[†] and Helmuth Möhwald[‡]

Institut de Chimie Séparative de Marcoule (ICSM), Bagnols sur Cèze, France, and Max Planck Institute of Colloids and Interfaces (MPIKGF), Potsdam, Germany

Received: May 20, 2010; Revised Manuscript Received: June 28, 2010

Power ultrasound (20 kHz, $I_{ac} = 20-56$ W cm^{-2}) was used to investigate physical and chemical effects of acoustic cavitation at the water−glass interface. Physical effects were characterized with different techniques of microscopy (optical, SEM, AFM) and were shown to increase and evolve as a function of sonication duration according to two distinctive periods: (i) an incubation period that initiates weak points on a glass surface, which may be the result of acoustically created shock-waves, and (ii) a second period of erosion, which is related to direct impact fracture erosion of the material. Chemical analysis of water (ICP-OES), after ultrasonic treatment, clearly indicates that bubble collapse at the water−glass interface initiates not only mechanical erosion but also accelerates the leaching processes of the glass components.

1. Introduction

The propagation of ultrasonic waves in a liquid medium may lead to acoustic cavitation, which is the formation, growth, and rapid implosive collapse of a vapor filled microbubble.[1,2] Rapid bubble implosion induces localized extreme conditions inside the bubble in terms of temperature and pressure ("hot spots") estimated to be about 5000 K and 0.1 GPa, respectively.[1,3–5] In addition, a part of the vaporized molecules can be dissociated to form radical species, such as OH$^{\bullet}$ and H$^{\bullet}$ for water sonolysis, then able to react rapidly in the middle.[6–9] These conditions are combined with a very fast cooling rate ($\sim 10^{10}$ K s^{-1}) and thus offer the opportunity of working at room temperature with extreme conditions.[3–5] When imploding in the vicinity of a solid boundary (heterogeneous cavitation), the bubble collapse becomes asymmetric and leads to a specific phenomenon: an inrush of liquid passes through the bubble, penetrates the opposite bubble interface, and strikes the surface with a high velocity (ca. few hundred meters per second). In addition, the collapse of the surrounding bubbles leads to the emission of shock waves supposed to reach a pressure of several GPa with a starting shock velocity of $\sim$4000 m s^{-1}.[10–14] These particular events, generally responsible for the occurrence of microdamages on sonicated surfaces, go with other effects (e.g., microstreamings and microturbulences) that will act together at the interface in different ways such as erosion, fusion, fragmentation, inclusion, etc.[1,5,15–18]

Among these broad effects, ultrasound-assisted cavitation erosion is a topic that attracted the attention of many scientists in view of the development of useful applications (cleaning, soldering, dentistry, extraction...). Cavitation erosion results in the repeated application of a high density of energy on a reduced zone of a treated surface.[19,20] This phenomenon generally causes an undesirable reduction of the lifetime of engine components dealing with fluids involved for industrial or engineering applications (ship propellers, pumps, valves, turbines, nozzles, etc.). High-power ultrasound constitutes a simple, reliable, and nonexpensive laboratory tool, allowing for testing of the resistance of materials and simulating the effects of hydrodynamic cavitation. Hence, acoustic cavitation was, for instance, implicated in the development and optimization of new coatings,[21,22] the study of the erosion resistance of metallic alloys,[23,24] the investigations of the cavitation erosion behavior of ceramics,[20,25] etc. Surprisingly, despite few papers dealing with metallic glasses,[26–28] the literature describing the influence of acoustic cavitation at the glass interface remains poorly described. To the best of our knowledge, we can only cite the work of Howard and Ball who used soda lime silica glass as a comparative specimen to investigate the cavitation erosion of titanium−aluminide-based alloys.[29] This study was performed for long periods of treatment and was not directly focused on the early stage of the erosion process. Nevertheless, glasses are interesting and useful models to study the cavitation erosion of ceramics because of their hardness, low porosity, and their relative immunity against chemical corrosion, which is known to increase cavitation damages.[25] In such circumstances, it is possible to study a reliable cavitation behavior of the material with a maximal avoidance of extraneous variables.

Up to date, the mechanisms of the processes involved during ultrasonic treatment of solid surfaces represent a topic that has not been totally clarified. Indeed, heterogeneous cavitation is a complex phenomenon where numerous parameters (saturating gas, intensity, temperature, etc.) require a careful tuning, and, besides, several factors may interfere during experimentation and play a critical role in the erosion process. Knapp et al. reported in 1955 that, during an acoustic cycle, only one of 30 000 bubbles is close enough to a solid surface to be able to create damages on it.[30,31] The attribution of the damages on a treated area appears nevertheless to result from the collapse of a cloud or cluster of bubbles, where the implosion of a single cavity may trigger and heighten the collapse of the neighboring bubbles (concerted collapse).[14,31–34] The shock loaded by the bubble collapse at the interface is strongly attenuated with the distance between the bubble wall and the solid surface. The implosion must happen at a distance smaller than twice the maximum radius of the bubble initially created.[11,12,35] Hence, a dimensionless stand-off parameter may be introduced: $\gamma =$

* Corresponding author. Phone: +33(0) 466 339 251. Fax: +33(0) 466 797 611. E-mail: serguei.nikitenko@cea.fr.
[†] ICSM.
[‡] MPIKGF.

10.1021/jp1046276
Published on Web 07/12/2010

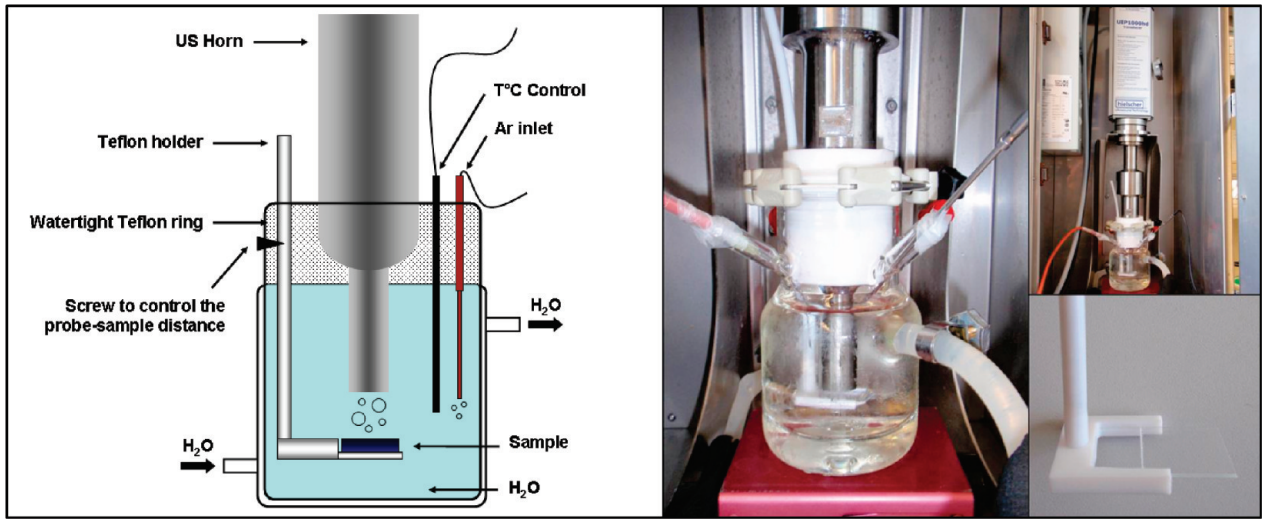

Figure 1. Homemade reactor and Teflon bar used during glass erosion experiments.

L/R_{max}, which is the ratio of the distance between the bubble center and the surface (L) and the bubble radius at its maximum size (R_{max}).[12,35] This parameter allows the investigation of reproducible experiments and finally permits the observation and classification of the effects loaded at the interface.[14,36] One can thereby admit that the surface itself may play a prevailing role in the erosion process: because of its characteristics (hardness, grains, heterogeneity, etc.), but also because of its influence on the surrounding collapsing bubbles (e.g., heterogeneous nucleation of a surface).

The aim of this Article is to contribute to the understanding of the phenomena and mechanisms involved in acoustic cavitation in aqueous solution at the solid−liquid interface. Two kinds of glasses, soda lime and fused silica, offering differences in composition and hardness, were studied under 20 kHz generated acoustic cavitation at the ultrasonic intensity of 20−56 W cm^{-2}. We intentionally investigated the early stage of the erosion process (incubation period and acceleration) with the aim of deciphering the mechanism of erosion for such a material. Furthermore, the influence of the glass surface hydrophobization on acoustic cavitation has been studied, a mechanism of erosion has been proposed, and an estimation of the energy delivered during the cavitation bubble collapse has been finally introduced.

2. Experimental Methods

2.1. Materials. Glass samples were optically smooth, devoid of apparent defects, and were visually examined before each experiment to eliminate samples showing eventual flaws. Before treatment, samples were kindly degreased and washed using ethanol then water. Soda lime glass samples were home prepared using standard glass microscopy slides (75 × 25 mm and about 1 mm thick, VWR, Darmstadt, Germany) by cutting them into pieces of 25 × 25 mm^2 in surface area. Fused silica glass (20 × 20 mm^2) samples were purchased from Laboratoire Chenu (Cournon d'Auvergne, France). The chemical composition of the involved materials (mol %) has been obtained with energy dispersive X-ray spectroscopy (Bruker SDD 5010) coupled with SEM FEI QUANTA 200 ESEM FEG (procedure and Table SI.1 described in the Supporting Information). Hydrophobization was done with octadecyldimethyl-chlorosilane as described in the Supporting Information. The experiments were performed in deionized milli-Q water prepared using a three-stage Millipore Milli-Q Plus 185 purification system, which had a resistivity higher than 18.2 MΩ cm, at 25 °C.

2.2. Ultrasonic Treatment. In typical experiments, glass samples were loaded on a home manufactured sample holder that allowed the sample to be held at a reproducible distance from the ultrasonic horn. This sample holder is Teflon made and allows a flat angle treatment of the sample with a 2 mm minimal distance between the probe and the sample (Figure 1). Holes previously created on the Teflon bar allowed us to screw the system and fix the distance by 3 mm increments. Sonochemical procedures were made using an UIP1000 hd ultrasonic processor (Hielscher GmbH, Teltow, Germany). The device comprises a piezoelectric transducer with a maximum peak-to-peak amplitude of 170 μm coupled with a booster and a titanium probe of 2.5 cm^2 immersed reproducibly below the surface of the sonicated water volume (250 mL). The maximal electrical power delivered to the device is 1000 W with a frequency of 20 kHz. The horn was fixed into a homemade reactor (Figure 1) using a watertight Teflon ring, and a cryostat purchased from FRYKA-Kältetechnik GmbH (KT06-42 400 W, Esslingen, Germany) was used to maintain the temperature of sonicated liquid.

Ultrasonic treatment was performed under an argon flow to ensure the maximal effect of cavitation. Argon was bubbled through the sonicated water with the rate of 100 mL min^{-1}, 10 min before sonication and during the whole sonication procedure. Specific acoustic power P_{ac} (W mL^{-1}) or ultrasonic intensity I_{ac} (W cm^{-2}) delivered to the solution was measured using the thermal probe method.[37] The hydrogen peroxide formation, created by the combination of hydroxyl radicals during water sonolysis under argon flow, has been measured as a chemical method of cavitation control.[7,38] The measured values were in the range 0.20−0.56 W mL^{-1} and 20−56 W cm^{-2} for specific acoustic power and acoustic intensity, respectively. Using an acoustic intensity of 20 W cm^{-2}, H_2O_2 production has been evaluated to be about 0.6 μM min^{-1}, which is in the same order of magnitude with published data found in the literature for a reactor with similar geometry.[38,39]

2.3. Mechanical Properties of Glasses. Nanoindentation was used to measure hardness (H) and Young's modulus (E) of glasses. A nanomechanical testing instrument (Ubi 1, Hysitron Inc., MN) has been used with a Berkovich diamond indenter tip (regular triangle pyramid geometry, ∼10 μm^2). The instrument has been calibrated using a fused quartz sample having an indentation modulus of 69.6 GPa. Indentations were performed in air at room temperature with an indenting orientation

of 90°. Each value thus obtained is a mean average of 12 indents. For each of them, the loading function used was as follows: 5 s loading, 2 s holding at 9000 μN, and 5 s unloading. H and E parameters were calculated using the software provided by the manufacturer. No cracks were observed around the indented area.

2.4. Erosion Evaluation − Physical Approach.

2.4.1. Microscopy. Optical microscopy was used for physical erosion quantification (see part 2.4.2 for explanations). Evaluations were made using a LEICA DMR equipped with a LEICA DFC480 CCD camera (Cambridge, Great Britain). Scanning electron microscopy (SEM) was used to observe and characterize the morphology of cavitation holes and eroded areas that appeared on glass surfaces after ultrasonic treatment. For analyses, samples were sputtered with platinum and measured using a Gemini Leo 1550 instrument (Carl Zeiss AG, Germany) at an operation voltage of 3.0 keV. Atomic force microscopy (AFM) was carried out to achieve topographic measurements and characterize the roughness, the height profile, and the created hole depths, of the sonicated surfaces. Measurements were surveyed in air at room temperature using a D3100 Nanoscope IIIa MultiMode microscope (Digital instruments/Veeco, Inc., Santa Barbara, CA) in tapping mode with silicon cantilevers (Nanoworld, Neuchâtel, Switzerland). Cantilevers have a typical resonance frequency of 285 kHz and a spring constant of 42 N m^{-1}. In this study, recorded images possess a scan area of 40 × 40 μm^2. Analyses and treatments of images were carried out with the software provided by the manufacturer.

2.4.2. Image Processing Software. Damage of ultrasonically eroded surfaces has been evaluated using an image processing software, "Image J".[40] After sonolysis, erosion of samples was checked using an optical microscope, and pictures of eroded areas were taken with a ×100 magnification. The saved pictures (256 gray levels, 8 bit mode) were then treated using the computer software in three steps: (i) background subtraction, to remove the defects brought by light exposure during microscopic measurements, (ii) binarization of the pictures via a threshold value of the gray level, to convert 256 bit images into 2 bit images (black and white images, coded 1 for black pixels and 0 for white pixels), and (iii) histogram evaluation of the proportion of black pixels in the entire picture seen as a pixel matrix. The described strategy is illustrated in Figure SI.1 shown in the Supporting Information. Such a procedure allowed generating pictures with damaged area clearly identified that can be described with eq 1.[13]

$$L = k^2 \sum_{i}^{I} \sum_{j}^{J} E(i,j) \text{ with } E(i,j) = 1 \text{ and } k = \sim 0.54\ \mu\text{m pixel}^{-1} \quad (1)$$

Dark regions in the resulting pictures thus correspond to the eroded areas and constitute the quantification mode of physical erosion effects. Image treatment was processed in batch mode, and the erosion of the sample was given as a percentage of eroded area per treated zone and derived from a mean of 10 pictures taken at various places on the sample.

2.5. Erosion Evaluation − Chemical Approach. After sonolysis, the liquid phases recovered from the reactor were directly filtered through a cellulose acetate 0.2 μm filter purchased from Whatman GmbH (Dassel, Germany). Analyses of bulk solutions were performed using inductively coupled plasma optical emission spectroscopy (ICP-OES) with a Spectro Arcos apparatus (Spectro Analytical Instruments GmbH, Germany) and equipped for axial plasma observation. Before injection, 9.8 mL of solution was diluted with 0.2 mL of HNO_3 to obtain a 2% acidified sample (∼0.3 M). The concentration of the targeted elements in solutions was checked against an external calibration curve prepared with certified standard solutions (Si, Na, Al, Ca) of 1000 μg mL^{-1} (SCP science, Courtaboeuf, France). Several wavelengths were studied during analyses; the measured lines were finally 589.592, 251.612, 396.847, and 396.152 nm, for Na, Si, Ca, and Al, respectively. The given values are a mean of three replicates.

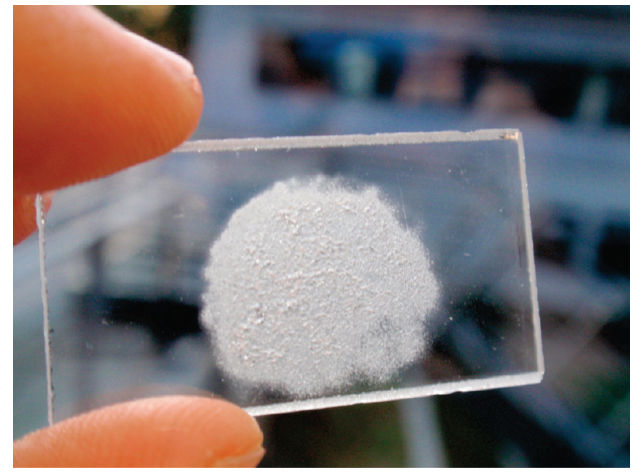

Figure 2. Erosion of fused silica glass sonicated during 180 min at 2 mm from the ultrasonic probe (I_{ac} = 49 W cm^{-2}).

3. Results and Discussion

3.1. Parameter Settings. Soda lime and fused silica glasses studied in this work offer the opportunity to study the effect of the material network on its cavitation resistance. Fused silica glass constitutes a kind of reference material because of its exclusive silicon oxide composition in amorphous form. This glass is constituted by a network of Si−O tetrahedra randomly distributed in the glass (Si−O−Si angle bond nonuniformity responsible for its noncrystalline structure). Each of the atoms are strongly bounded to each other (covalent bonds), resulting in a strong material with a very low thermal expansion and very high thermal shock resistance. On the opposite, soda lime glass is an amorphous material presenting concentrations of network modifiers such as Na_2O (13.19%) or CaO (7.06%). The presence of sodium and calcium disrupts the network by creating nonbridging oxygen ions (ionic bonds). The resulting structure is more open than fused silica glass, and presents bigger rings and a decreased number of Si−O bonds.[41] Also note here the presence of Al_2O_3 (1.76%) in silica lime glass whose concentration was followed during chemical investigations to characterize the behavior of another glass former component.

The dramatic effect generated after 3 h of ultrasonic treatment (I_{ac} = 49 W cm^{-2}) focused on a fused silica glass sample is shown in Figure 2. The influence of variables such as the probe−sample distance, the applied acoustic intensity, and the sonication duration was studied at the first stage to establish the parameters that allow glass erosion. These studies reveal that cavitation erosion is highly dependent on the probe−sample distance (see the Supporting Information, Figure SI.2a). When the distance between the probe and the glass is increasing, the erosion drops dramatically. A 2 mm distance was thus chosen for the rest of the experiments. The experiments also show that cavitation erosion effects are strongly dependent on the acoustic intensity in the range of 20−56 W cm^{-2}. Erosion effects increase

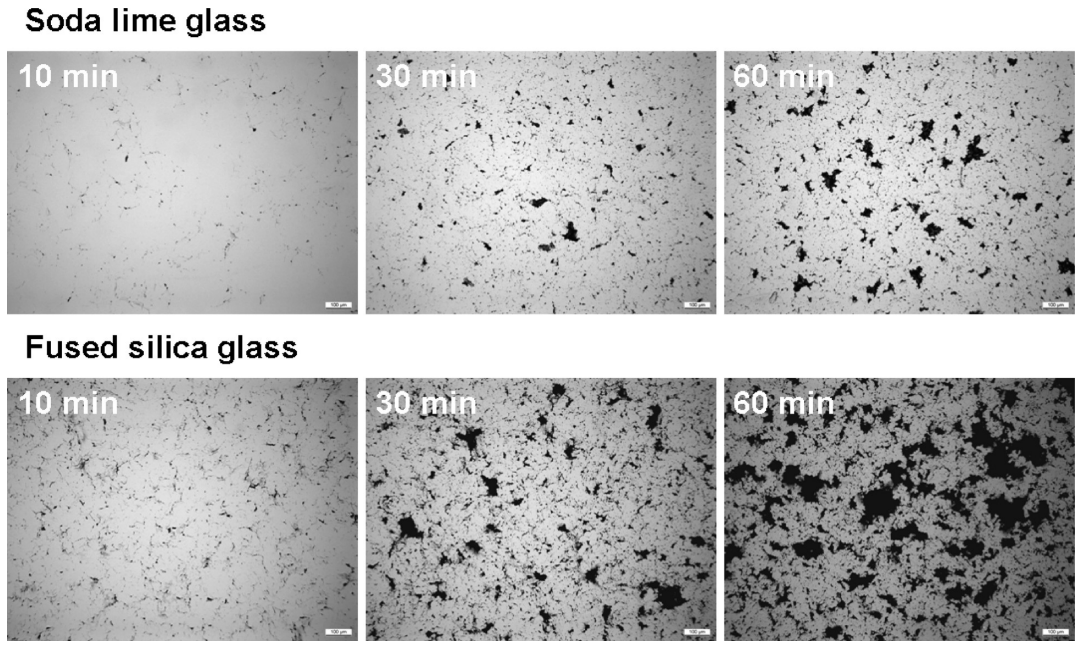

Figure 3. Optical microscope observation of soda lime and fused silica glass surfaces as a function of sonication time (I_{ac} = 49 W cm^{-2}).

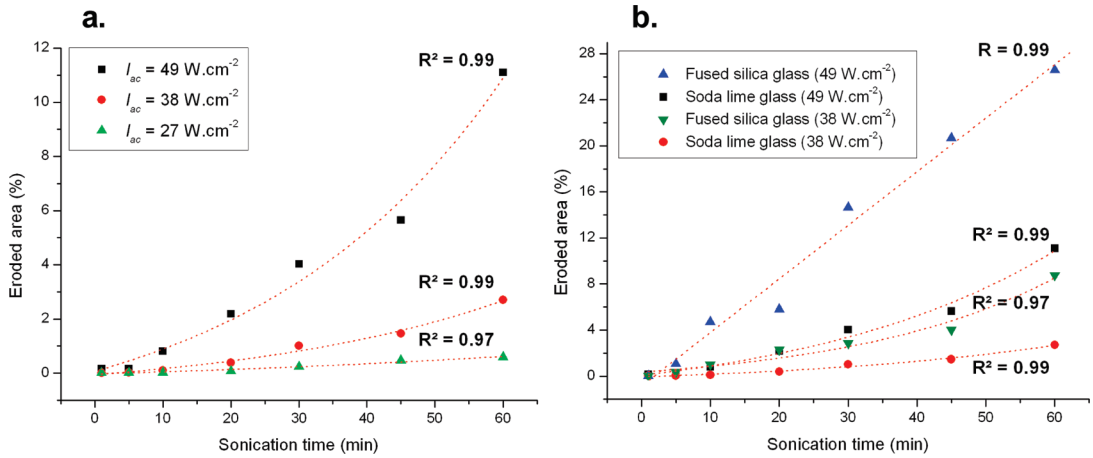

Figure 4. (a,b) Erosion profile of sonicated (I_{ac} = 27, 38, and 49 W cm^{-2}) soda lime glass as a function of sonication time (a), and comparison with fused silica glass for sonication at I_{ac} = 49 and 38 W cm^{-2} (b). R and R^2 are the correlation coefficients obtained for the profiles fitted with a linear or an exponential equation, respectively.

with ultrasonic intensity until a threshold of 49 W cm^{-2} and are decreasing thereafter (Figure SI.2b of the Supporting Information). Such an effect has been already observed by Whillock et al. during the study of ultrasound-induced corrosion of stainless steel.[42] They attributed the presence of this maximum to a peak in the cavitation intensity, which is supposed to increase with applied acoustic intensity as long as the collapse time allows the cavity to grow. In another way, an increase of the applied acoustic intensity could also enhance the number of acoustic bubbles between the horn and the sample. The effects thus appearing at the interface (e.g., microturbulences and microstreamings) may then be increased and play a screening effect that inhibits cavitation erosion.[43]

3.2. Physical Characterization of the Erosion. The effects of cavitation erosion observed with optical microscopy at I_{ac} = 49 W cm^{-2} are illustrated in Figure 3 for different times of sonication. The combination of optical microscopic observations with the image processing software allowed us to characterize a two-dimensional evolution of the studied surfaces as a function of sonication duration (Figure 4a and b). Erosion of the surface increases with sonication time and applied acoustic intensity for soda lime glass as well as for fused silica. The observed erosion for soda lime glass was found to be well fitted with an exponential function of the kind: $Y = Y_0 + Ae^{t/x}$, where Y is the percentage of eroded area and t is the sonication duration (min). Erosion rate values, calculated as the derivative of the fitting curve ($\partial Y/\partial t$) for the various intensities, are summarized in Table 1. The erosion rate increase, combined with the exponential shape of the erosion curves, demonstrate the autocatalytic character of the soda lime glass cavitational erosion. Such kind of behavior has been already pointed out in the literature dealing with cavitation erosion and is generally described as an incubation period that leads to a bigger and more quantifiable erosion rate.[19,25,26] SEM measurements (Figure 5) allowed us to characterize the erosion incubation period of soda lime glass by the presence of small primary cavities at the surface (~1−2 μm). These cavities are differing from plastic deformation ("pits"), generally described in the literature as responsible for erosion phenomena, and attributed to microjet impingements.[13,44] The primary cavities observed on soda lime glass can be associated with the generation of microcracks as well (primary effects of cavitation) and result in a negligible

TABLE 1: Erosion Rate ($mm^2\ min^{-1}$) as a Function of Sonication Duration (38 and 49 W cm^{-2}) for the Different Treated Surfaces, Reported for the 2.5 cm^2 Area of the Ultrasonic Probe

	soda lime glass ($mm^2\ min^{-1}$)		fused silica glass ($mm^2\ min^{-1}$)		silanized glass ($mm^2\ min^{-1}$)	
time (min)	38 W cm^{-2}	49 W cm^{-2}	38 W cm^{-2}	49 W cm^{-2}	38 W cm^{-2}	49 W cm^{-2}
10	0.063	0.236	0.148	1.165	0.048	0.198
30	0.103	0.406	0.291	1.165	0.058	0.281
60	0.221	0.920	0.792	1.165	0.080	0.469

loss of material (low loss of mass weight). The second period of erosion is related to a direct loss of material and refers to the erosion of larger particles with a diameter generally bigger than 10 μm that tends to overlap and accelerate the erosion process.

The damaged areas created during the incubation period constitute zones of nucleation. As a matter of fact, these primary areas of erosion (cavities and microcracks) act by themselves as nucleation sites, facilitating the formation of bubbles, and thus promoting the erosion of the surface.[13,45] The generation of new acoustic bubbles is more easily done (increase of the erosion rate as a function of time), and transient bubbles then collapse at one "acoustic cycle distance" from the nucleation site and create an accumulation of impact areas. These effects lead finally to the interconnection of cracks[46] that "draw" the shape of bigger damaged zones, which are removed from the surface with the increase of sonolysis duration. This explains the shape of the erosion curve and finally supports the idea of clustering of cavitation erosion effects where each new eroded area is dependent on the previously damaged zone. This clusterization behavior, accelerating the erosion rate, has already been described in the literature.[13,26,47] For instance, Dular and Osterman described the pit clustering evolution created by means of ultrasound on a thin aluminum foil.[13]

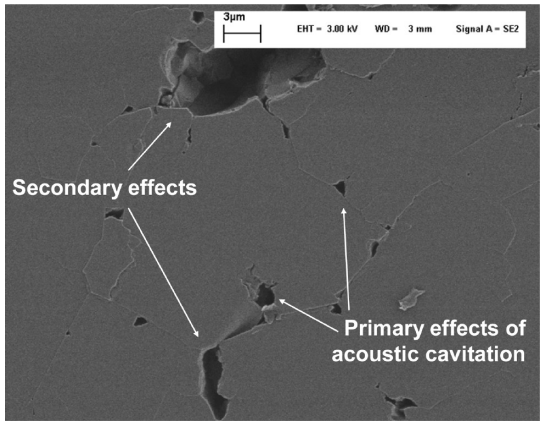

Figure 5. SEM observation of soda lime glass after 15 min of sonication (I_{ac} = 49 W cm^{-2}) at a 2 mm distance from the ultrasonic probe.

AFM topographic measurements presented in Figure 6 reveal that the erosion damages are more pronounced for fused silica than for soda lime glass, which is in line with the kinetic data of erosion. Soda lime glass appears to be much more resistant than fused silica glass whatever the applied acoustic intensity or the duration of sonolysis. The erosion profile of fused silica glass for I_{ac} = 38 W cm^{-2} was found to be well fitted with the same exponential function described for soda lime glass (Figure 4b). On the other hand, the cavitation erosion profile of fused silica glass submitted to an acoustic intensity of 49 W cm^{-2} was found to be best fitted with a linear regression. The application of this linear model implies an erosion profile that can vary with the applied acoustic intensity. The linear model lacks an incubation period. Actually, the erosion profiles of materials are supposed to operate in several steps: incubation period, acceleration period, and steady-state period. In the experimental range studied, the cavitation erosion resistance of fused silica glass may be not strong enough to display the incubation and acceleration periods. Calculated rates of erosion are significantly higher for fused silica than those for soda lime glass (Table 1).

The surface roughness of fused silica glass appears clearly more pronounced whatever the sonication time. The evolution of surface roughness for ultrasonically treated samples was quantified using two parameters: the arithmetic average of the absolute values of the surface height deviations measured from the mean plane, R_a, and the root-mean-square average of height deviations taken from the mean image data plane, R_q. These

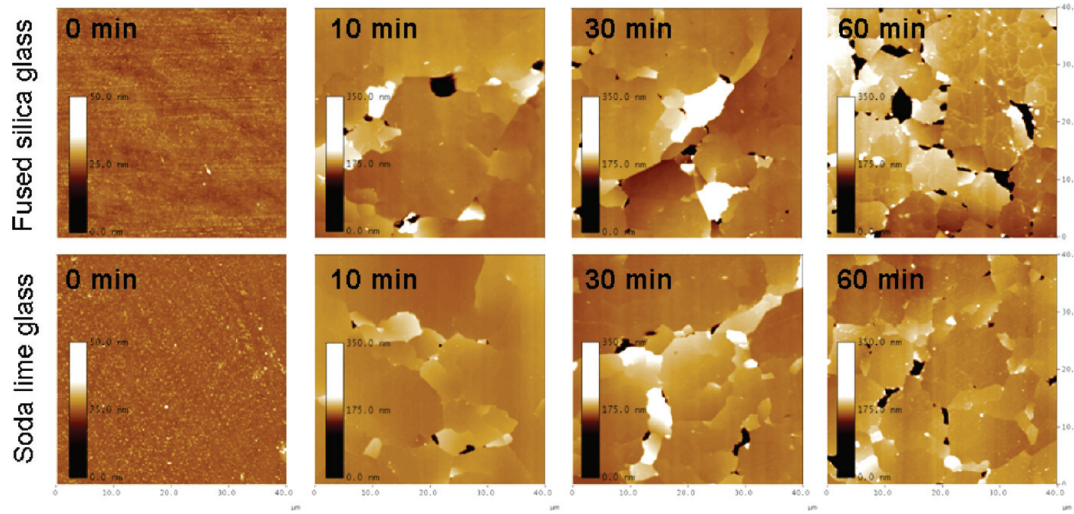

Figure 6. AFM topographic measurements of glass surfaces for different times of sonication at I_{ac} = 38 W cm^{-2} (vertical legends are for surface height).

TABLE 2: Time Evolution of Roughness ($n > 10$) for Sonicated Specimens

	soda lime glass		fused silica glass	
sonication (min)	R_a (nm)	R_q (nm)	R_a (nm)	R_q (nm)
0	1.67 ± 0.61	2.50 ± 0.73	0.97 ± 0.21	1.62 ± 0.71
10	5.19 ± 2.30	11.44 ± 5.63	11.25 ± 3.46	28.03 ± 6.58
30	9.39 ± 2.99	25.52 ± 15.53	11.20 ± 3.51	27.39 ± 6.36
60	12.39 ± 4.24	33.92 ± 12.04	35.52 ± 7.09	90.67 ± 18.50

parameters were obtained from AFM data according to the following equations:

$$R_a = \frac{1}{N}\sum_{j=1}^{N}|Z_j| \quad (2)$$

$$R_q = \sqrt{\frac{\sum Z_i^2}{N}} \quad (3)$$

Table 2 demonstrates that surface roughnesses are in a nanometer range before ultrasonic treatment for both materials. The parameter R_a increases rapidly with sonication time and is much more important for fused silica glass than that for soda lime glass. The same observation arises with the R_q parameter for both materials. The roughness of fused silica glass is more significant, thus reinforcing its lower cavitation erosion resistance. While roughness values are still increasing for fused silica glass after 60 min of ultrasonic treatment, measurements made for soda lime glass indicate that its roughness tends to reach a plateau, which is in agreement with the observations on the cavitation erosion resistance of soda lime glass (observations done when tracing the curves with values of Table 2; see the Supporting Information, Figure SI.3). The diameters and depths of the cavities resulting from acoustic cavitation were measured ($n > 25$) after 10 min for both samples and are summarized in Table 3. The size difference between cavities is not obvious. Slightest values may be pointed out for fused silica glass, but the difference is not important enough to permit a discrimination between the observed effects. That observation is in good agreement with the erosion profiles described earlier where the incubation periods are similar for both materials.

Surprisingly, the erosion rates determined for each of the involved materials were inversely proportional to their measured hardness H (Tables 1 and 3), which is a parameter often considered as a good erosion resistance index.[14,48] This parameter expresses the resistance of a material to permanent deformation. A good correlation between cavitation erosion resistance of bulk metallic glasses and their initial respective hardness was, for instance, reported by Drozdz et al.[26] In our study, material presenting the lowest hardness gives the higher cavitation erosion resistance. The same observation rises with elasto-plastic indexes, which are parameters often associated with hardness to predict erosion behavior.[48–50] H/E (elasticity index or elastic strain to failure parameter) and H^3/E^2 (resistance to plastic deformation) were thus not correlated with involved specimens.

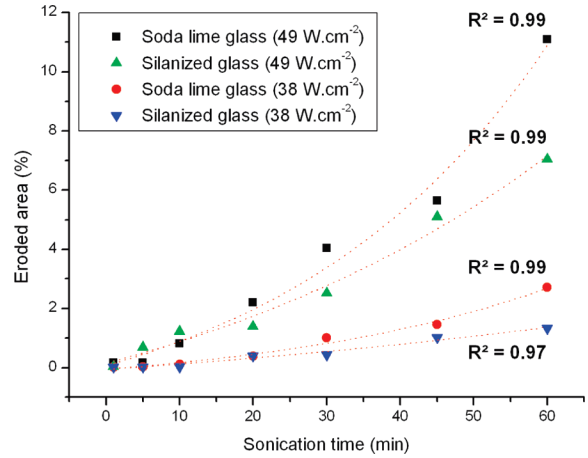

Figure 7. Cavitation erosion profile (I_{ac} = 49 and 38 W cm^{-2}) of hydrophobized glass against soda lime glass as a function of sonication time. R^2 is the correlation coefficient obtained for the fitted exponential equations.

The lack of significance of these parameters suggests the absence of a plastic fracture mode. Nevertheless, the erosion behavior of studied glass samples was found to be in good agreement with the brittleness index (B), which corresponds to the ratio between hardness (resistance to deformation) and toughness (resistance to fracture).[51,52] Thus, brittleness index (B) is a good parameter to express whether a material tends to fracture into a ductile or a brittle mode. The absence of correlation between hardness (or plasticity indexes) with erosion behavior of a surface has already been described in the literature.[53,54] Besides, an increase of the H/E ratio may imply a change from a plastic to a brittle fracture mode, which is in agreement with the literature and our investigations.[29,48,54] It can be thus concluded that the cavitation erosion resistance of glass under acoustic cavitation is governed by the brittleness index. In other words, the harder is the glass, the less resistant under acoustic cavitation it is. However, the more brittle is the glass, the easier is the erosion under acoustic cavitation.

3.3. Effect of Glass Silanization. Hydrophobized soda lime glasses were submitted to acoustic cavitation using the same treatment procedure. The physical erosion comparison of hydrophobic (water contact angle ~90.6°) and hydrophilic surfaces (water contact angle ~54.3°) indicates comparable erosion profiles whatever the acoustic intensity (Figure 7). The incubation periods are almost identical for both materials, but the erosion rates associated with the secondary effects are slightly lower for the hydrophobized sample as compared to hydrophilic glass (Table 1). One can conclude that the silanization of soda lime glass surface causes the increase of its cavitation erosion resistance. Microscopic images of eroded glass specimens presented in the Supporting Information (Figure SI.4) confirm this observation. These discrepancies could be interpreted by two hypotheses: (i) the silanization procedure causes the decrease of the initial surface roughness due to the surface defect smoothing, or (ii) hydrophobization may change the distance of the imploding microbubbles by moving them closer to the boundary. That implies a modification of the dimensionless stand-off parameter $\gamma = L/R_{max}$ (ratio between the

TABLE 3: Mechanical Properties of Sonicated Materials ($n = 12$), and Average Measurements for the Diameter and Depth of Holes (Primary Effects of Cavitation) from the Initial Period of Erosion ($n > 25$)

glass specimen	E_r (GPa)	H (GPa)	H/E_r	H^3/E_r^2 (GPa)	B (μm$^{-1/2}$)	hole diameter (μm)	hole depth (nm)
soda lime	68.64	6.23	0.091	0.051	8.2[52]	1.79 ± 0.56	203.9 ± 45.6
fused silica	66.13	8.68	0.131	0.150	10.0[52]	1.73 ± 0.41	191.0 ± 58.9

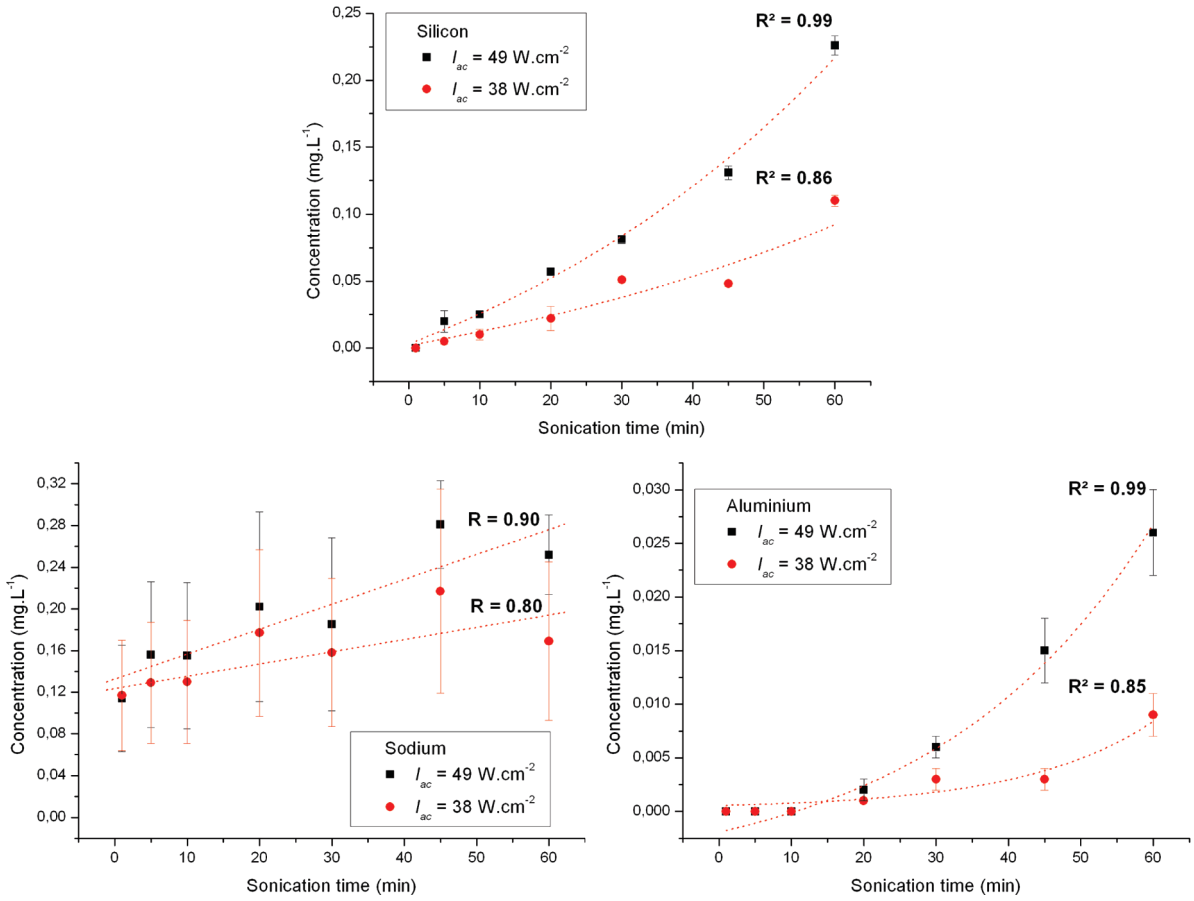

Figure 8. Concentration evolution of the measured elements (Si, Na, Al) for soda lime glass as a function of sonication time and applied acoustic intensity (I_{ac} = 49 and 38 W cm^{-2}). R and R^2 are the correlation coefficients of the concentration profiles fitted with a linear or an exponential equation, respectively.

surface−bubble center distance and the radius of the bubble at its maximum size). Such a modification involves an erosion mechanism that may differ from the one involved in the nonsilanized surface.[12,14]

3.4. Chemical Characterization of the Erosion. Kinetic curves of Si, Na, and Al solubilization for eroded soda lime glass are shown in Figure 8. The concentration profiles of Si and Al can be well fitted with the exponential function $Y = Y_0 + Ae^{t/x}$, where Y is the concentration and t is the sonication time, which is similar to that observed for the erosion profiles. The evolution of elements in water during sonication is summarized in Tables SI.2 and SI.3 of the Supporting Information. The concentration of Na in solution appears to be roughly equivalent to the concentration of Si, while its concentration in glass is much smaller than that of Si (see the Supporting Information, Table SI.1). This might be the result of a faster release of network modifiers than network formers during the sonication procedure. Furthermore, calculations of Si/Al ratio, as a function of sonolysis time, indicate an accumulation of Al increasing faster than that observed for Si (in comparison with original glass composition). This indicates a noncongruent release of glass elements under acoustic cavitation. Surprisingly, sonicated solution is more concentrated in Si for soda lime glass than for fused silica glass, while its cavitation erosion resistance was shown to be much stronger. The open structure displayed by soda lime glass, with larger network rings, and a decreased connectivity (in comparison with fused silica glass) may explain its lower chemical resistance during sonolysis.[41]

3.5. Glass Erosion Mechanism. According to the literature, ultrasound-assisted erosion of surfaces is generally attributed to two principal effects: microjets and shock-waves.[2,12−14,16,47] However, our results show that microjet impingements do not appear as a valuable factor explaining the erosion of glass surfaces. Indeed, microjets are inrushes of liquid that hit the surface with a velocity estimated to be about several hundred meters per second.[12,20,44] The water hammer pressure P, exerted by the microjet at the impact zone, can be expressed as: $P = \rho c v$, where P is the resulting pressure, ρ is the density of the liquid, c is the velocity of sound in the medium, and v is the velocity of the microjet at the impinged surface.[16,20,34] Considering an average microjet velocity of ∼150 m s^{-1}, with a velocity of sound in water of ∼1500 m s^{-1} and a water density of ∼1000 kg m^{-3}, one can calculate the maximal pressure roughly exerted by the microjet at the interface. In this case, the calculated pressure is ∼0.225 GPa. Such kind of microjets is able to produce enough peak pressure during a short pulse to initiate some pits on soft metals and ductile materials (e.g., aluminum, steel, nickel, iron, etc.).[13,21,47,55] However, this pressure is too low to initiate cracks and cavities on brittle materials such as studied glasses.

On the other hand, although the amplitude of shock wave pressure is known to decrease rapidly with the surface−bubble wall distance,[10,11] high speed photography recently allowed the estimation of the pressure produced by a collapsing bubble (1.08 MHz), situated at 68 μm from the surface, to be around 1.3 GPa.[11] Extrapolating these data, the authors estimated the pressure acting on the bubble wall to be ∼7.7 GPa. The pressure propagated around the cavitation bubble, estimated from single bubble sonoluminescence data at 20 kHz, was found by other authors to be in the range of 4−6 GPa.[10] In this study, the

measured hardness for soda lime and fused silica glasses was equal to 6.23 and 8.68 GPa, respectively. Therefore, the peak pressure developed by microjets is not sufficient to reach the level of materials' hardness needed to imply the glass rupture. Their effects appear secondary, while the energy involved in shock-waves is susceptible to reach pressure levels situated in the hardness range of the studied specimens.

From our point of view, shock waves are the main causes of ultrasound-assisted erosion of glass surfaces, particularly during the incubation period. Indeed, the incubation period presents a primary erosion of the surface, which results in a slight but measurable loss of material in contrast to plastic deformation. A combination of microjets, shock waves, microstreamings, and microturbulences is then probably involved during the second period of erosion that includes the propagation of cracks, cleaning of the surface, detachment of particles, etc. Particle collisions with the surface may also be involved. A good description of the various forces (shear forces, lift forces, drag forces, attraction forces, etc.) acting on a surface to remove adsorbed particles has been given by Maisonhaute et al.[43] Even if shock wave attenuation occurs very fast during its propagation, the hardness measurement goes with the brittle fracture mode highlighted previously. The behavior of glass surfaces under acoustic cavitation excludes microjets, as potentially responsible for plastic deformation of ductile materials.

Following these observations, the quantity of energy delivered at the interface during the bubble collapse can be roughly estimated. For instance, the hardness of fused silica glass, measured with nanoindentation, was found to be equal to 8.68 GPa corresponding to an energy density of $\sim 8.68 \times 10^{10}$ J m^{-3}. Assuming a conical shape of the primary effects of cavitation, and using the data presented in Table 3, the average volume of material removed from glass after each impact at the primary stage of erosion can be estimated as $\sim 1.50 \times 10^{-19}$ m^3. Assuming that one primary cavity is created due to one impact of collapsing bubble, the energy delivered by one bubble is deduced to be about $\sim 13.02 \times 10^{-9}$ J/bubble, or ~ 5.54 mJ mm^2 in terms of energy density at the glass surface for an average area of primary holes around 2.35 μm^2 (Table 3). This value appears to be about 10-fold higher than the energy densities generated in shock wave therapy for treatment of calcifying tendinitis.[56–58] On the other hand, it is about 8-fold smaller than the typical energy density of shock waves generated by a CO_2 laser pulse during enhanced breakdown emission spectroscopy.[59]

4. Conclusion

This Article contributes to the understanding of the mechanisms involved at the solid−liquid interface under 20 kHz sonication, in aqueous solution. Physical and chemical effects resulting from ultrasound-induced erosion on glass surfaces were characterized with various techniques (optical microscopy, AFM, MEB, ICP-OES) and were shown to evolve and to be highly dependent on experimental settings (distance, acoustic intensity, sonication time, hardness of surfaces, etc.). The developed chemical approach, by measurements of the release of elements contained in the glass as a function of sonication parameters and materials, provides an attractive way of investigating ultrasound-assisted erosion, generally described as a function of weight loss. Hence, the physical and chemical effects of ultrasound at the interface are clearly highlighted. The results showed that a correlation between both effects is not obvious (fused silica glass exhibits a better chemical durability, while its cavitation erosion resistance is lower). Furthermore, connecting the physicochemical erosion effects with an estimation of the energy distributed at the interface supports the proposed erosion mechanism and yields quantitative information. Hence, this investigation gives a better knowledge and a solid basis to deal with the behavior of glass materials under acoustic cavitation.

Acknowledgment. This study, supported by CNRS, France, was carried out within the framework of the "Laboratoire Européen Associé SONO", which links the skills of research from ICSM Marcoule and MPI Potsdam-Golm. We gratefully acknowledge Tatiana Borodina, Dmitriya Borisova, Anneliese Heilig, Jürgen Krägel, Petra Leibner, and Renaud Podor for help in experiments and useful discussions. M.V. thanks CEA/DEN for a postdoctoral fellowship.

Supporting Information Available: Additional figures and tables, with an improved description of the materials and methods used for the study. This material is available free of charge via the Internet at http://pubs.acs.org.

References and Notes

(1) Mason, T. J.; Lorimer, J. P. *Applied Sonochemistry: Uses of Power Ultrasound in Chemistry and Processing*; Wiley-VCH Verlag GmbH & Co. KGaA: New York, 2002.

(2) Mason, T. J.; Riera, E.; Vercet, A.; Lopez-Buesa, P. Application of Ultrasounds. *Emerging Technologies for Food Processing*; Elsevier Ltd.: New York, 2005.

(3) Suslick, K. S.; Didenko, Y.; Fang, M. M.; Hyeon, T.; Kolbeck, K. J.; McNamara, W. B.; Mdleleni, M. M.; Wong, M. Acoustic Cavitation and its Chemical Consequences. *Philos. Trans. R. Soc., A* **1999**, *357*, 335–353.

(4) Suslick, K. S. In *Encyclopedia of Physical Science and Technology*, 3rd ed.; Meyers, R. A., Ed.; Academic Press: San Diego, CA, 2001.

(5) Suslick, K. S.; Price, G. J. Applications of Ultrasound to Materials Chemistry. *Annu. Rev. Mater. Sci.* **1999**, *29*, 295–326.

(6) Riesz, P.; Berdahl, D.; Christman, C. L. Free Radical Generation by Ultrasound in Aqueous and Nonaqueous Solutions. *Environ. Health Perspect.* **1985**, *64*, 233–252.

(7) Nikitenko, S. I.; Venault, L.; Moisy, Ph. Scavenging of OH Radicals Produced from H_2O Sonolysis with Nitrate Ions. *Ultrason. Sonochem.* **2004**, *11*, 139–142.

(8) Mišík, V.; Riesz, P. Free Radical Formation by Ultrasound in Organic Liquids: a Spin Trapping and EPR Study. *J. Phys. Chem.* **1994**, *98*, 1634–1640.

(9) Cravotto, G.; Cintas, P. Power Ultrasound in Organic Synthesis: Moving Cavitational Chemistry from Academia to Innovative and Large-Scale Applications. *Chem. Soc. Rev.* **2006**, *35*, 180–196.

(10) Pecha, R.; Gompf, B. Microimplosions: Cavitation Collapse and Shock Wave Emission on a Nanosecond Time Scale. *Phys. Rev. Lett.* **2000**, *84*, 1328–1330.

(11) Brujan, E. A.; Ikeda, T.; Matsumoto, Y. On the Pressure of Cavitation Bubbles. *Exp. Therm. Fluid Sci.* **2008**, *32*, 1188–1191.

(12) Leighton, T. G. The Acoustic Bubble. *Effects and Mechanisms*; Academic Press: London, 1994; Chapter 5.

(13) Dular, M.; Osterman, A. Pit Clustering in Cavitation Erosion. *Wear* **2008**, *265*, 811–820.

(14) Karimi, A.; Martin, J. L. Cavitation Erosion of Materials. *Int. Met. Rev.* **1986**, *31*, 1–26.

(15) Prozorov, T.; Prozorov, R.; Suslick, K. S. High Velocity Interparticle Collisions Driven by Ultrasound. *J. Am. Chem. Soc.* **2004**, *126*, 13890–13891.

(16) Kuppa, R.; Moholkar, V. S. Physical Features of Ultrasound-Enhanced Heterogeneous Permanganate Oxidation. *Ultrason. Sonochem.* **2010**, *17*, 123–131.

(17) Radziuk, D.; Grigoriev, D.; Zhang, W.; Su, D.; Möhwald, H.; Shchukin, D. Ultrasound-Assisted Fusion of Preformed Gold Nanoparticles. *J. Phys. Chem. C* **2010**, *114*, 1835–1843.

(18) Radziuk, D.; Möhwald, H.; Shchukin, D. Ultrasonic Activation of Platinum Catalysts. *J. Phys. Chem. C* **2008**, *112*, 19257–19262.

(19) Franc, J. P.; Michel, J. M. *Fundamentals of Cavitation (Fluid Mechanics and Its Applications)*; Kluwer Academic Publishers: Springer, 2004; Chapter 12: Cavitation Erosion.

(20) Lu, J.; Zum Gahr, K.-H.; Schneider, J. Microstructural Effects on the Resistance to Cavitation Erosion of ZrO_2 Ceramics in Water. *Wear* **2008**, *265*, 1680–1686.

(21) Lampke, T.; Dietrich, D.; Leopold, A.; Alisch, G.; Wielage, B. Cavitation Erosion of Electroplated Nickel Composite Coatings. *Surf. Coat. Technol.* **2008**, *202*, 3967–3974.

(22) Münsterer, S.; Kohlhof, K. Cavitation Protection by Low Temperature TiCN Coatings. *Surf. Coat. Technol.* **1995**, *74*−*75*, 642–647.

(23) Lee, M. K.; Hong, S. M.; Kim, G. H.; Kim, K. H.; Rhee, C. K.; Kim, W. W. Numerical Correlation of the Cavitation Bubble Collapse Load and Frequency with the Pitting Damage of Flame Quenched Cu-9Al-4.5Ni-4.5Fe Alloy. *Mater. Sci. Eng., A* **2006**, *425*, 15–21.

(24) Di Vernieri Cuppari, M. G.; Wischnowski, F.; Tanaka, D. K.; Sinatora, A. Correlation Between Microstructure and Cavitation-Erosion Resistance of High Chromium Cast Steel - Preliminary Results. *Wear* **1999**, *225*−*229*, 517–522.

(25) Niebuhr, D. Cavitation Erosion Behaviour of Ceramics in Aqueous Solutions. *Wear* **2007**, *263*, 295–300.

(26) Drozdz, D.; Wunderlich, R. K.; Fecht, H.-J. Cavitation Erosion Behaviour of Zr-Based Bulk Metallic Glasses. *Wear* **2007**, *262*, 176–183.

(27) Tamura, S.; Tsunekawa, Y.; Okumiya, M.; Hatakeyama, M. Ultrasonic Cavitation Treatment for Soldering on Zr-Based Bulk Metallic Glass. *J. Mater. Proc. Technol.* **2008**, *206*, 322–327.

(28) Roper, G. W. Cavitation Erosion Resistance of Metglas Alloy 2826 MB. *J. Mater. Sci. Lett.* **1984**, *3*, 674–676.

(29) Howard, R. L.; Ball, A. Mechanisms of Cavitation Erosion of Ti-Al-Based Titanium Aluminide Intermetallic Alloys. *Acta Mater.* **1996**, *44*, 3157–3168.

(30) Knapp, R. T. Recent Investigations of the Mechanics of Cavitation and Cavitation Damage. *Trans. Am. Soc. Mech. Eng.* **1955**, *77*, 1045–1054.

(31) Vyas, B.; Preece, C. M. Stress Produced in a Solid by Cavitation. *J. Appl. Phys.* **1976**, *47*, 5133–5138.

(32) Hansson, I.; Morch, K. A. The Dynamics of Cavity Clusters in Ultrasonic (Vibratory) Cavitation Erosion. *J. Appl. Phys.* **1980**, *51*, 4651–4658.

(33) Pishchalnikov, Y. A.; Sapozhnikov, O. A.; Bailey, M. R.; Williams, J. C.; Cleveland, R. O.; Colonius, T.; Crum, L. A.; Evan, A. P.; McAteer, J. A. Cavitation Bubble Cluster Activity in the Breakage of Kidney Stones by Lithotripter Shockwaves. *J. Endourol.* **2003**, *17*, 435–446.

(34) Bourne, N. K. On the Collapse of Cavities. *Shock Waves* **2002**, *11*, 447–455.

(35) Philipp, A.; Lauterborn, W. Cavitation Erosion by Single Laser-Produced Bubbles. *J. Fluid Mech.* **1998**, *361*, 75–116.

(36) Minsier, V.; De Wilde, J.; Proost, J. Simulation of the Effect of Viscosity on Jet Penetration into a Single Cavitating Bubble. *J. Appl. Phys.* **2009**, *106*, 1–10.

(37) Hagenson, L. C.; Doraiswamy, L. K. Comparison of the Effects of Ultrasound and Mechanical Agitation on a Reacting Solid-Liquid System. *Chem. Eng. Sci.* **1998**, *53*, 131–148.

(38) Nikitenko, S. I.; Le Naour, C.; Moisy, Ph. Comparative Study of Sonochemical Reactors with Different Geometry Using Thermal and Chemical Probes. *Ultrason. Sonochem.* **2007**, *14*, 330–336.

(39) Chave, T.; Nikitenko, S. I.; Granier, D.; Zemb, T. Sonochemical Reactions with Mesoporous Alumina. *Ultrason. Sonochem.* **2009**, *16*, 481–487.

(40) *ImageJ*; U.S. National Institutes of Health, Bethesda, MD; http://rsb.info.nih.gov/ij/.

(41) Alexander, C. S.; Chhabildas, L. C.; Reinhart, W. D.; Templeton, D. W. Changes to the Shock Response of Fused Quartz Due to Glass Modification. *Int. J. Impact Eng.* **2008**, *35*, 1376–1385.

(42) Whillock, G. O. H.; Harvey, B. F. Ultrasonically Enhanced Corrosion of 304L Stainless Steel: The Effect of Frequency, Acoustic Power and Horn to Specimen Distance. *Ultrason. Sonochem.* **1997**, *4*, 33–38.

(43) Maisonhaute, E.; Prado, C.; White, P. C.; Compton, R. G. Surface acoustic cavitation understood via nanosecond electrochemistry. Part III: shear stress in ultrasonic cleaning. *Ultrason. Sonochem.* **2002**, *9*, 297–303.

(44) Dular, M.; Bachert, B.; Stoffel, B.; Širok, B. Relationship Between Cavitation Structures and Cavitation Damage. *Wear* **2004**, *257*, 1176–1184.

(45) Verdan, S.; Burato, G.; Comet, M.; Reinert, L.; Fuzellier, H. Structural Changes of Metallic Surfaces Induced by Ultrasound. *Ultrason. Sonochem.* **2003**, *10*, 291–295.

(46) Adjouadi, N.; Laouar, N.; Bousbaa, C.; Bouaouadja, N.; Fantozzi, G. Study of Light Scattering on a Soda Lime Glass Eroded by Sandblasting. *J. Eur. Ceram. Soc.* **2007**, *27*, 3221–3229.

(47) Haosheng, C.; Jiang, L.; Darong, C.; Jiadao, W. Damages on Steel Surface at the Incubation Stage of the Vibration Cavitation Erosion in Water. *Wear* **2008**, *265*, 692–698.

(48) Krella, A.; Czyøniewski, A. Investigation Concerning the Cavitation Resistance of Tin Coatings Deposited on Austenitic Stainless Steel at Various Temperatures. *Wear* **2008**, *265*, 72–80.

(49) Guruvenket, S.; Azzi, M.; Li, D.; Szpunar, J. A.; Martinu, L.; Klemberg-Sapieha, J. E. Structural, Mechanical, Tribological, and Corrosion Properties of a-SiC:H Coatings Prepared by PECVD. *Surf. Coat. Technol.* **2010**, 204, 3358−3365.

(50) Leyland, A.; Matthews, A. On the Significance of the H/E Ratio in Wear Control: a Nanocomposite Coating Approach to Optimised Tribological Behaviour. *Wear* **2000**, *246*, 1–11.

(51) Lawn, B. R.; Marshall, D. B. Hardness, Toughness, and Brittleness: an Indentation Analysis. *J. Am. Ceram. Soc.* **1979**, *62*, 347–350.

(52) Le Bourhis, E. *Glass: Mechanics and Technology*; Wiley-VCH Verlag GmbH & Co. KGaA: New York, 2008; Chapter 8.2: Sharp Contact Resistance.

(53) Lima, M. M.; Godoy, C.; Modenesi, P. J.; Avelar-Batista, J. C.; Davison, A.; Matthews, A. Coating Fracture Toughness Determined by Vickers Indentation: an Important Parameter in Cavitation Erosion Resistance of WC-Co Thermally Sprayed Coatings. *Surf. Coat. Technol.* **2004**, *177*−*178*, 489–496.

(54) Krella, A. The Influence of TiN Coatings Properties on Cavitation Erosion Resistance. *Surf. Coat. Technol.* **2009**, *204*, 263–270.

(55) Wu, C. Z.; Chen, Y. J.; Shih, T. S. Phase Transformation in Austempered Ductile Iron by Microjet Impact. *Mater. Charact.* **2002**, *48*, 43–54.

(56) Magosch, P.; Lichtenberg, S.; Habermeyer, P. Radial Shock Wave Therapy In Calcifying Tendinitis Of The Rotator Cuff-A Prospective Study. *Z. Orthop. Ihre Grenzgeb.* **2003**, *141*, 629–636.

(57) Jakobeit, C.; Winiarski, B.; Jakobeit, S.; Welp, L.; Spelsberg, G. Ultrasound-Guided, High Energy Extracorporeal Shock-Wave Treatment of Symptomatic Calcareous Tendinopathy of the Shoulder. *ANZ J. Surg.* **2002**, *72*, 496–500.

(58) Cosentino, R.; Selvi, E.; De Stefano, R.; Frati, E.; Manca, S.; Hammoud, M.; Marcolongo, R. Extracorporeal Shock Wave Therapy for Chronic Calcific Tendinitis of the Shoulder. *Clin. Rheumatol.* **2004**, *23*, 475–477.

(59) Killinger, D. K.; Allen, S. D.; Waterbury, R. D.; Stefano, C.; Dottery, E. L. Enhancement of Nd:YAG LIBS emission of a remote target using a simultaneous CO_2 laser pulse. *Opt. Express* **2007**, *15*, 12905–12915.

JP1046276